Interface Debonding in Fiber Reinforced Cement-Matrix Composites

M. SHANNAG*
Civil Engineering Dept.
Jordan University of Science and Technology
P.O. Box 3030
Irbid 22110 Jordan

W. HANSEN AND P. TJIPTOBROTO
Civil Engineering Dept.
University of Michigan
Ann Arbor, MI 48109

(Received August 11, 1997)
(Revised January 16, 1998)

ABSTRACT: Shear lag theory was used to predict the extent of fiber debonding at the end of the elastic range in a high performance Fiber Reinforced Concrete (FRC) such as DSP (Densified Small Particles). The analysis predicts two-way debonding at onset of first cracking in FRC's containing randomly distributed, discrete steel fibers. Findings indicate that the extent of fiber debonding at first cracking is relatively low for DSP containing fiber volume fractions higher than 3% when compared to ordinary FRC containing fiber volume fractions less than 1%. This analysis allows a more accurate prediction of elastic strain in FRC's.

KEY WORDS: concrete, FRC, shear lag, elastic tensile strain capacity, debonding.

INTRODUCTION

RECENT RESEARCH HAS shown that the mechanical properties of fiber reinforced cementitious composites depend strongly upon the nature of the fiber-matrix interface. The interface plays an important role as a medium for shear stress transfer between the fibers and the matrix, and in energy dissipation mechanisms during composite fracture [1–5]. Many researchers have attempted to predict the overall composite response based on the constitutive equations of the interface and the matrix crack properties [6–10]. However, most of these equations do not pro-

*Author to whom correspondence should be addressed.

0021-9983/99/02 0158–19 $10.00/0

vide accurate prediction of composite response, and they do not always agree [8,9,11]. Composite failures in cementitious composites usually initiate as matrix cracking and interface debonding. Aveston and Kelly [6] have indicated that in many composite systems, the appearance of the first crack in the matrix will lead to some debonding at the interface between the fiber and the matrix. They have derived mathematical expressions for estimating the extent of debonding in glass fiber reinforced cement systems. These expressions depend highly on the ratio between the shear strength of the interface and the matrix cracking strength. Tjiptobroto [12] has indicated that the effect of partial fiber debonding on elastic strain prediction is pronounced at high fiber volume fractions in fiber reinforced DSP cement. Leung and Li [13] have shown that the fiber-matrix interface debonding energy plays an important role as an additional means for significant energy absorption in high performance FRC's containing high fiber volume fractions. Recently, using the Moire interferometry technique, Shao, Li, and Shah [14] have shown that the interface is not completely debonded even when the composite is loaded to very high strains (more than four times as large as the strain corresponding to the one when the multiple cracking has stopped).

This study investigates the phenomenon of partial fiber debonding at first cracking. Using shear lag theory [10,8,9,15,16], a new analytical expression was developed to predict the interface debonding in FRC composites. The magnitude of fiber debonding at the onset of cracking was determined and included in a micromechanical model used for predicting the elastic tensile strain of FRC composites containing randomly distributed discrete fibers. The present investigation leads to a better and improved design of composites containing high fiber volume fractions.

EXTENT OF DEBONDING AT ONSET OF CRACKING

When a composite undergoes tensile loading, it can be shown that a slight increase in the debonded surface of the fibers at onset of cracking causes a significant increase in the energy absorbed at the fiber-matrix interface, and vice versa. The magnitude of fiber debonding length before and after first cracking can be used to estimate the extent of fiber debonding at the onset of cracking. Mathematical expressions rely on shear lag theory [10] and on certain assumptions used to calculate the debonding length before and after cracking. Once the debonded length is computed, the corresponding change in the debonding energy can be determined and incorporated in a micromechanical model used to predict the tensile strain capacity of the composite.

Before Onset of Cracking

The debonded length before onset of cracking can be determined using Equation (1). The boundary condition of zero normal stress at the end of the fiber is applied to

determine the constants B and D. Equation (1) is then differentiated to get the elastic interfacial stress τ_{el}. Finally, the resulting expression is equated to the maximum elastic interfacial strength of the composite. These steps are shown below.

The stress in the fiber up to the end of elastic region [10] is given by Equation (1).

$$\sigma_f = E_f \varepsilon_{mu} + B \sinh\left(\frac{nx}{r}\right) + D \cosh\left(\frac{nx}{r}\right) \tag{1}$$

where σ_f, E_f, r are fiber stress, modulus, and radius respectively.

x: distance from fiber mid-point
ε_{mu}: composite strain = matrix strain

$$n = \sqrt{\frac{E_m}{E_f(1+\nu_m)\ln\dfrac{R}{r}}} \tag{2}$$

where
E_m = modulus of elasticity of the matrix
ν_m = Poisson's ratio of the matrix
R = median distance between fibers

$$R = \frac{1}{2}\sqrt{\frac{\pi d^2}{V_{ef}}} \tag{3}$$

For square packing of fibers, where V_{ef} is the effective fiber volume fraction (i.e. half of the nominal value of fiber volume fraction).

$$\ln\left(\frac{R}{r}\right) = \frac{1}{2}\ln\left(\frac{\pi}{V_{ef}}\right) \tag{4}$$

B and D are constants determined from the boundary conditions at the ends of the fiber where the normal stress is zero. Therefore, Equation (1) becomes

$$\sigma_f = E_f \varepsilon_{mu} \left\{ 1 - \frac{\cosh\left(\dfrac{nx}{r}\right)}{\cosh(ns)} \right\} \tag{5}$$

From force equilibrium at a section of a fiber:

$$d\sigma_{\phi} = -\frac{\tau_{el}}{r} dx \tag{6}$$

where τ_{el} is the elastic interfacial stress.

Differentiating Equation (5) and multiplying the result by $(-r/2)$:

$$\tau_{el} = -\frac{r}{2}\frac{d\sigma_f}{dx} = -\frac{r}{2}\left[-nE_f\varepsilon_{mu}\frac{\sinh\left(\frac{nx}{r}\right)}{\cosh(ns)} \right] \tag{7}$$

$$\tau_{el1}(x) = \frac{1}{2}nE_f\varepsilon_{mu}\left[\frac{\sinh\left(\frac{nx}{r}\right)}{\cosh(ns)} \right] \tag{8}$$

where τ_{el} is the elastic interfacial stress before cracking.

The value of debonded length before cracking (L_{db1}) can be determined by setting $\tau_{el\,1}(\max)$ = interfacial strength of material.

Thus

$$\frac{1}{2}nE_f\varepsilon_{mu}\left[\frac{\sinh\left(\frac{nx}{r}\right)}{\cosh(ns)} \right] = \tau_{el}(\max) \tag{9}$$

Solve for x to get the initial debonded length L_{db1}.

Figure 1(a) shows the distribution of the interfacial shearing stress and the debonded length L_{db1} before the onset of cracking.

After Onset of Cracking

The debonded length after onset of cracking can be determined in a similar way to that used before onset of cracking. This determination can be made with different boundary conditions and with the assumption that the fiber ends are bonded to the matrix. Figure 2 shows that the effect of different fiber embedded lengths is taken into account through the assumption

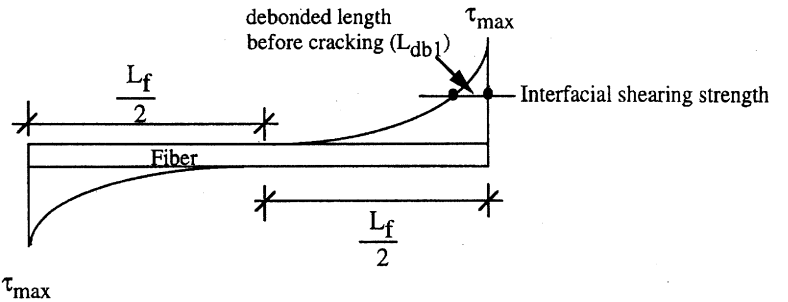

(a) Just before cracking (One-way debonding)

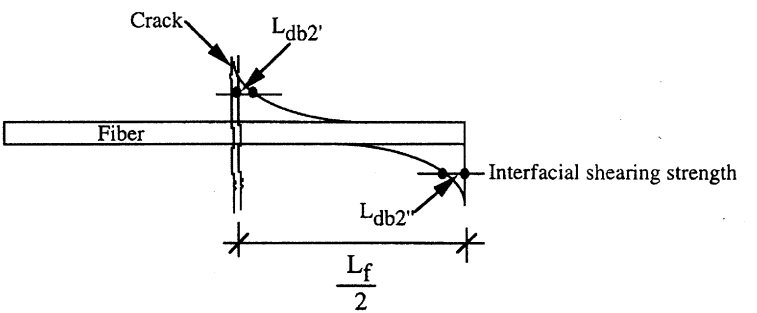

debonded length after cracking= $L_{db2} = L_{db2'} + L_{db2''}$

(b) Just after cracking (Two-way debonding)

Figure 1. *Typical distribution for the elastic interfacial stress at onset of cracking for FRC.*

of average strain values in the matrix and the fiber. The steps carried out are shown below.

If the elastic bond between the fiber and the matrix is still prevailing at the interface, σ_f can be described using the expression based on the shear lag theory [10] as given by Equation (1):

$$\sigma_f = E_f \varepsilon_{mu} + B \sinh\left(\frac{nx}{r}\right) + D \cosh\left(\frac{nx}{r}\right)$$

The constants B and D can be determined from the boundary conditions of the average strain in the fiber at first cracking as shown in Figure 2 [17].

Solving for B and D:

$$B = \frac{\alpha E_f \varepsilon_{mu}\left(\frac{1}{2} - \cosh\left(\frac{nl}{d}\right)\right)}{\sinh\left(\frac{nl}{d}\right)} \tag{10}$$

$$D = E_f \varepsilon_{mu} \alpha \tag{11}$$

Substitute for B and D in Equation (1):

$$\sigma_f = E_f \varepsilon_{mu} + \frac{\alpha E_f \varepsilon_{mu}\left(\frac{1}{2} - \cosh\left(\frac{nl}{d}\right)\right)}{\sinh\left(\frac{nl}{d}\right)} \sinh\left(\frac{nx}{r}\right) + \alpha E_f \varepsilon_{mu} \cosh\left(\frac{nx}{r}\right) \tag{12}$$

The interfacial stress can be obtained by differentiating Equation (12) and multiplying by $(-r/2)$. From force equilibrium:

$$\tau_{el} = -\frac{r}{2}\frac{d\sigma_f}{dx}$$

$$= \left[\frac{\alpha E_f \varepsilon_{mu}\left(\frac{1}{2} - \cosh\left(\frac{nl}{d}\right)\right)}{\sinh\left(\frac{nl}{d}\right)} \cosh\left(\frac{nx}{r}\right) * \frac{n}{r} + \alpha E_f \varepsilon_{mu} \sinh\left(\frac{nx}{r}\right)\right] \times \left(-\frac{r}{2}\right) \tag{13}$$

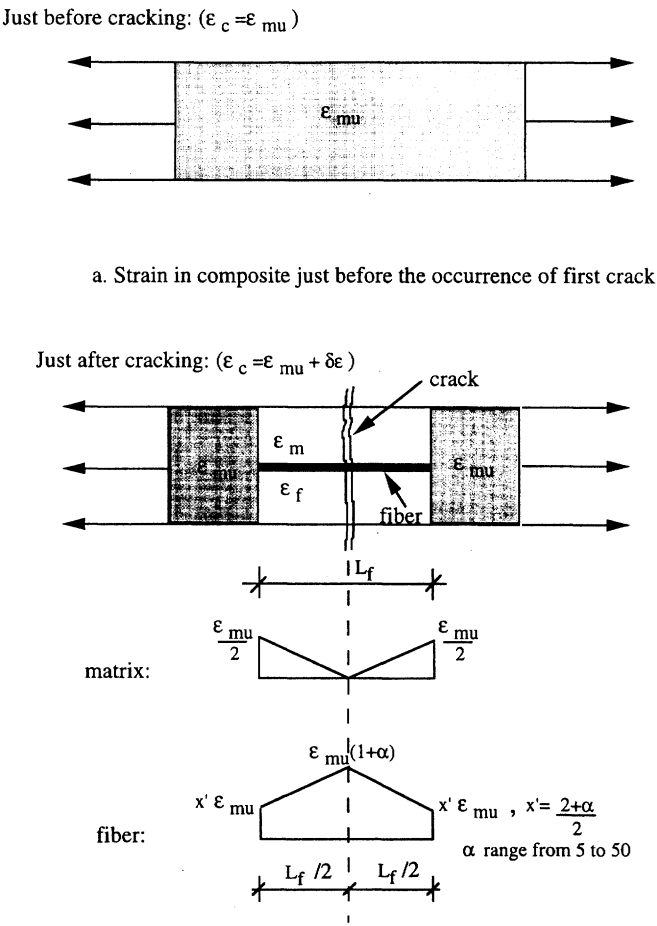

Figure 2. *Assumptions used in shear lag analysis [17].*

$$\tau_{el2}(x) = \frac{1}{2} nE_f \varepsilon_{mu} \left[\frac{\cosh(ns) - \frac{1}{2}}{\sinh(ns)} \cosh\left(\frac{nx}{r}\right) - \sinh\left(\frac{nx}{r}\right) \right] \quad (14)$$

where τ_{el2} is the elastic interfacial stress after onset of cracking. The debonded length just after the first crack L_{db2} can be determined by setting:

$$\tau_{el2}(x) = \tau_{frictional} \quad (15)$$

$$\frac{1}{2} n\alpha E_f \varepsilon_{mu} \left[\frac{\cosh(ns) - \frac{1}{2}}{\sinh(ns)} \cosh\left(\frac{nx}{r}\right) - \sinh\left(\frac{nx}{r}\right) \right] = \tau_{frictional} \quad (16)$$

Solve for x to get the debonded length just after cracking L_{db2}.

Figure 1(b) shows the distribution of the interfacial shearing stress and the debonded length L_{db2} just after the onset of cracking.

Energies of Fiber Debonding

It is well known that the tensile strain and toughness of FRC's are highly dependent on the properties of the fiber/matrix interfacial zone. In this study the elastic and the frictional bond strengths of the interface for ordinary mortar and high performance DSP were determined through single fiber pullout tests that employ a specially-designed apparatus [18,19].

The energies associated with fiber debonding and friction up to complete debonding were also estimated and listed in Table 1. These energies were derived from a simplified model given in Reference [11]. A typical output of a single fiber pullout test for the composite system investigated is shown in Figure 3.

To simulate the actual tensile behavior of the composite containing high fiber volume fractions of randomly distributed short steel fibers, 6 mm long and 0.15 mm in diameter, the interfacial properties of steel fibers embeded in a composite with similar properties were determined and listed in Table 1. Within the range of the fiber embedment lengths used in pullout experiments [18,19], the frictional and elastic bond strengths were almost identical and varied from 4.9 to 6.8 MPa for high performance DSP, and 1.8 to 2.8 MPa for ordinary mortar. The debonding and frictional energies up to complete fiber debonding have shown an increase with the increase in fiber embedment length and ranged from 57 to 210 Nm/m^2 for DSP and 18 to 40 Nm/m^2 for ordinary mortar.

Table 1. Input parameters used in shear lag analysis.

Material DSP	L_f (mm)	Shearing Stress		Debonding Energy (Nmm)	Frictional Energy (Nmm)	Elastic Strain Energy (Nmm)	Total Energy (Nmm)	Debonding and Frictional Energy (Nm/m^2)
		Frictional (MPa)	Elastic (MPa)					
	6	6.67	6.77	0.049	0.154	0.154	0.357	56.67
	12	5.81	5.82	0.218	0.843	0.843	1.904	148.11
	18	4.89	4.96	0.402	1.855	1.855	4.113	210.04
Ordinary FRC								
	6	2.71	2.79	0.011	0.053	0.053	0.116	17.87
	12	1.75	1.8	0.03	0.112	0.112	0.254	19.82
	18	1.95	1.95	0.082	0.345	0.345	0.772	39.74

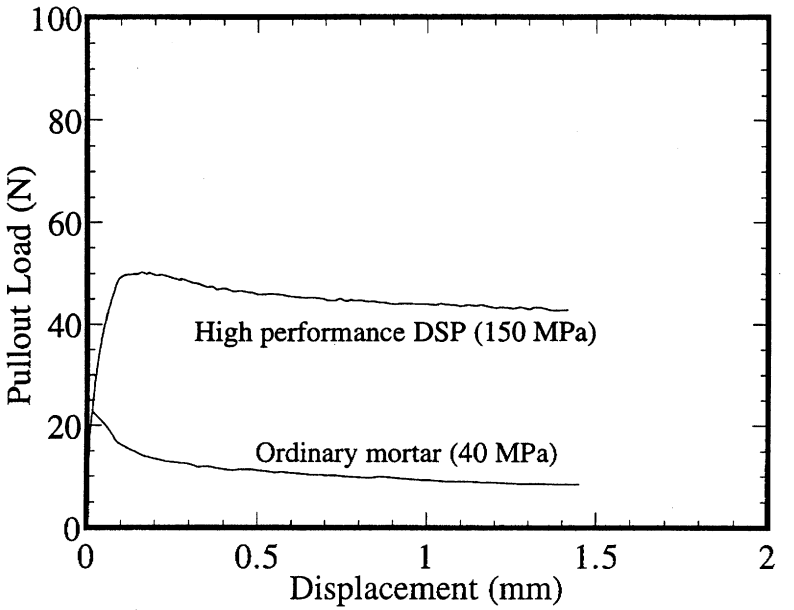

Figure 3. *Typical pullout curves for high performance DSP and ordinary mortar (fiber diameter = 0.19 mm, embedded length = 18 mm).*

The matrix cracking (elastic) strain values used in the shear lag analysis were predicted by the elastic strain model [17], and verified from flexure experiments carried out in a previous study [12]. The elastic moduli of the steel fiber and the DSP and mortar matrices were also experimentally determined in References [18,19]. For steel fibers, the elastic modulus was 200 GPa and 49 GPa for the DSP matrix and 21 GPa for the ordinary mortar matrix.

Elastic Strain Prediction

The equation for predicting the approximated elastic strain ε_{mu} for FRC's containing discrete discontinuous randomly distributed fibers is shown below. It is assumed that no fiber debonding has occurred at first cracking, and the transfer length is equal to half the fiber length [12].

$$\varepsilon_{mu} \approx \sqrt{\frac{2\gamma_m V_m}{\left[\frac{3}{4}E_c - \frac{7}{24}E_f V_{ef}(1+\alpha)\right]\alpha\beta L_f}} \tag{17}$$

where:

ε_{mu} is the elastic strain of the composite
V_{ef} is the effective fiber volume fraction, (i.e., half of the nominal value of fiber volume fraction).
γ_m is the matrix surface energy
L_f is the fiber length
E_f is the modulus of elasticity of the fiber
E_m is the modulus of elasticity of the matrix
E_c is the modulus of elasticity of the composite

$$\alpha = \frac{E_m V_m}{E_f V_{ef}} \tag{18}$$

$$\beta = \frac{L_{tr}}{L_f/2} \tag{19}$$

L_{tr} is the fiber transfer length

$$L_{tr} = \frac{d_f \sigma_f}{4\tau} \tag{20}$$

σ_f is the fiber stress after cracking

$$\sigma_f = \varepsilon^*_{mu}(1+\alpha)E_f \tag{21}$$

ε^*_{mu} is the approximated elastic strain [Equation (17) without β]

$$\varepsilon^*_{mu} = \sqrt{\frac{2\gamma_m V_m}{\left[\frac{3}{4}E_c - \frac{7}{24}E_f V_{ef}(1+\alpha)\right]\alpha L_f}} \tag{22}$$

d_f is the fiber diameter
τ is a constant frictional interfacial stress

Effect of Partial Fiber Debonding on Composite Elastic Strain

At high fiber fractions (i.e. > 3%), partial fiber debonding may occur because of high strain values. The extent of debonding was estimated from shear lag analysis. The effect of partial fiber debonding was included as an approximation in the model derivation with the addition of the change in the interface debonding energy (ΔU) because of the change in fiber debonded length as shown by Equation (23).

$$\varepsilon_{mu1} = \sqrt{\frac{2\gamma_m V_m + \Delta U}{\left[\frac{3}{4}E_c - \frac{7}{24}E_f V_{ef}(1+\alpha)\right]\alpha\beta L_f}} \tag{23}$$

Change of Interfacial Debonding Energy at Onset of Cracking

In this study the change in the debonding energy was estimated by knowing the debonded length at the onset of cracking (just before and after the occurrence of the first crack).

The total debonding energy for cylindrical fibers [12] is given by:

$$U = \frac{V_f}{\pi r^2} * 2\pi r * \frac{L_f}{4} * G_i * 2 \tag{24}$$

where G_i is the interface debonding energy per unit crack area

$$U = \frac{V_f L_f G_i}{r} \tag{25}$$

The change in the total debonding energy of the interface varies linearly with the change in fiber debonded length before and after cracking, [12], as given by Equation (26).

$$\Delta U = \frac{\Delta L_{db} U}{L_f} \tag{26}$$

$$\Delta L_{db} = 2(L_{db2} - L_{db1}) \tag{27}$$

where

L_{db1} is the debonded length before cracking
L_{db2} is the debonded length after cracking
ΔL_{db} is the change in the debonded length

RESULTS AND DISCUSSION

The debonding behavior of fibers strongly affects the properties of fiber-reinforced composites. Analysis of fiber pullout test results indicated that the frictional and debonding energies shown in Table 1 play a major part in the determination of the tensile strain capacity of the composite. Table 1 shows that the fiber pullout energies increase with the increase in fiber embedment length. This may be caused by further extension in the size of the fracture process zone at the crack tip and larger embedded surface area of the fiber [23].

Use of the shear lag analysis shown previously, and the input parameters presented in Table 1, made possible the determination of the change in the fiber debonded length at the onset of cracking. The total change in the frictional and debonding energies along the debonded length of the fiber were computed and incorporated as an approximation in the elastic strain model for a better prediction of the strain, as given by Equation (23).

The variation of the interfacial shearing stress with distance from the fiber midpoint, at onset of cracking, for DSP and ordinary FRC systems is shown in Figures 4 and 5. The shearing stress distributions shown in this investigation were similar to those published recently by Shoe et al. [14] who obtained their results by using the experimental Moire interferometry technique. The composites investigated contain up to 12% fiber volume fraction of short (6 mm long and 0.15 mm diameter) steel fibers randomly distributed within the matrix.

Figures 4 and 5 show that once the interfacial shear strength of the composite is reached, fiber debonding occurs. The extent of fiber debonding is highly dependent on the interfacial shearing strength and fiber volume fraction. The interfacial shearing strength is largely related to matrix cracking strength.

Before onset of cracking, the interfacial shear stress reaches a maximum value at the loaded end of the fiber, as shown in Figures 4(a) and 5(a), a phenomenon known in the literature as one-way debonding [10,12,13,20,21]. The debonded length of the fiber before onset of cracking increases with increase in fiber volume, as shown in Figure 6. This increase may be caused by the high strain values associated with incorporating high fiber volume fractions within the matrix.

After onset of cracking, the interfacial stress distribution has local maxima at the ends of the fiber, as shown in Figures 4(b) and 5(b). This distribution indicates that debonding could occur simultaneously at the loaded and embedded ends of the fiber. This phenomenon leads to the two-way debonding case proposed by Leung and Li [13]. The debonded length of the fiber after cracking decreases with the increase in fiber volume fraction, as shown in Figure 6. This decrease may occur because the cracking load is shared by many fibers.

Figure 6 indicates that the change in the debonded length of the fiber at the onset of cracking decreases by half when increasing the fiber volume fraction increases from 3 to 12%. This change indicates that incorporating high fiber volume frac-

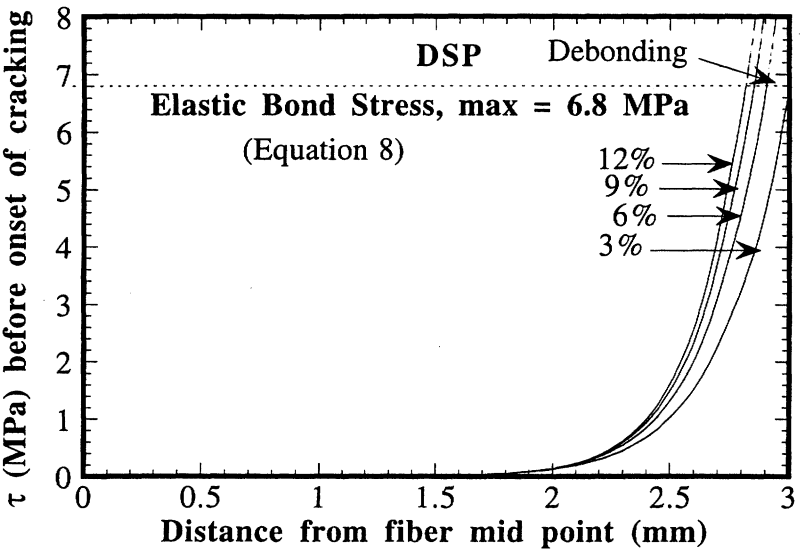

Figure 4a. *Interfacial shear stress distribution before onset of cracking for high performance DSP.*

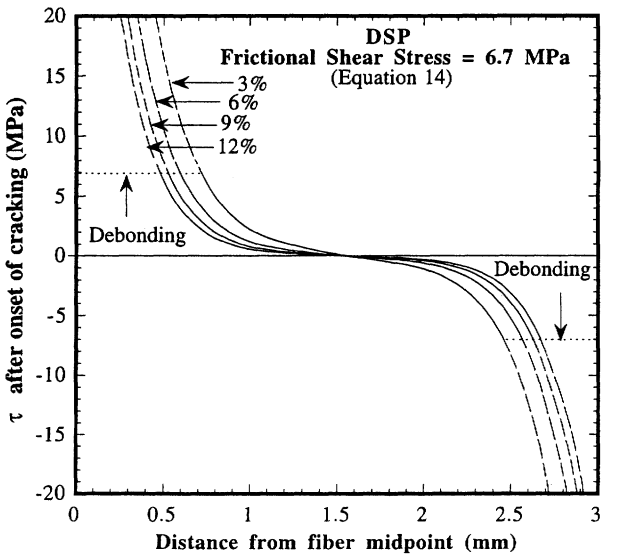

Figure 4b. *Interfacial shear stress distribution after onset of cracking for high performance DSP.*

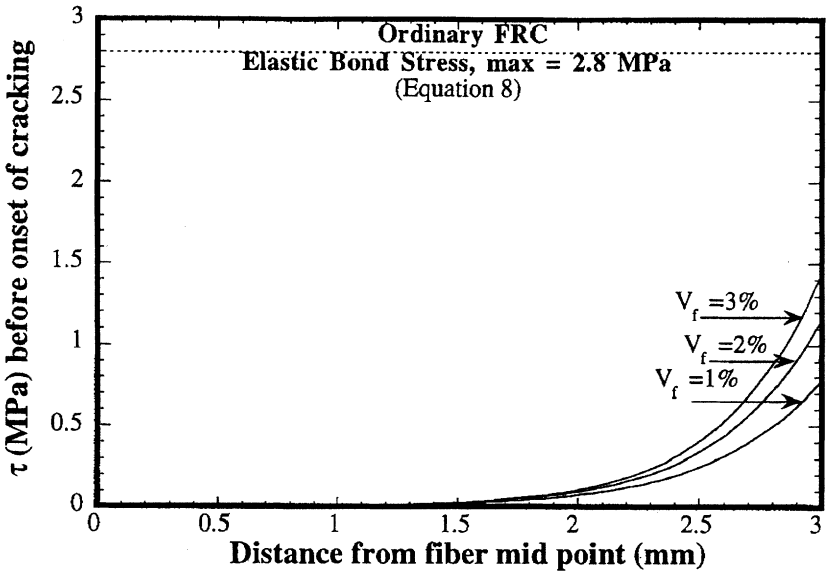

Figure 5a. *Interfacial shear stress distribution before onset of cracking for ordinary FRC.*

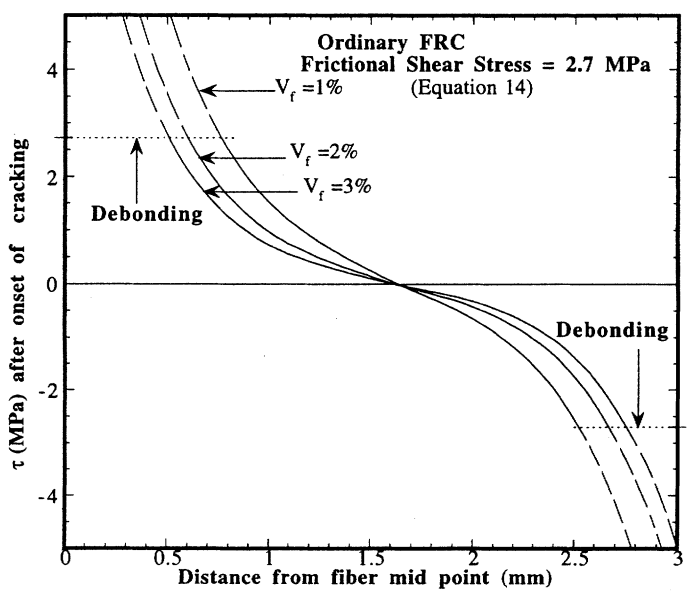

Figure 5b. *Interfacial shear stress distribution after onset of cracking for ordinary FRC.*

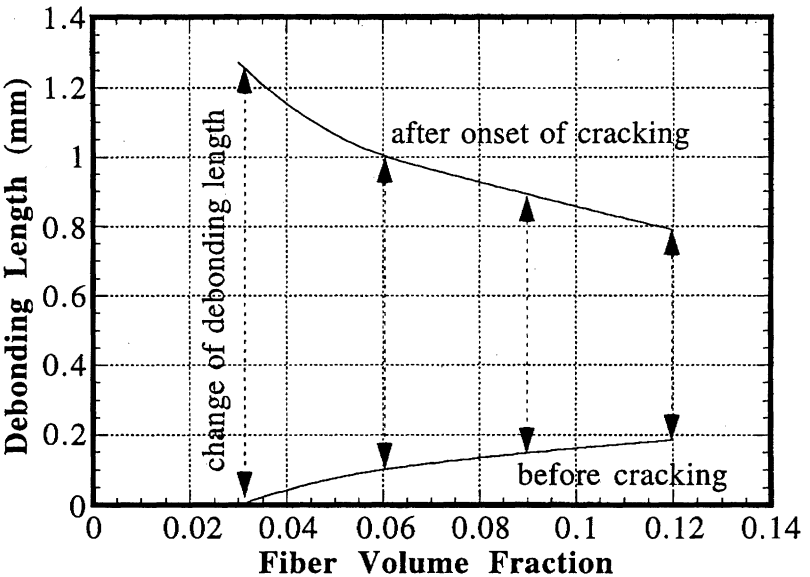

Figure 6. *Change in fiber debonded length at onset of cracking for DSP.*

tions in DSP matrix enhances the occurrence of multiple cracking because of less fiber debonding.

The occurrence of one-way or two-way debonding is related to the assumptions shown in Figure 2 with regard to the strain distribution at the ends of the fiber. This distribution is a function of matrix cracking strain and α which is highly dependent on the fiber volume fraction and matrix/fiber moduli ratio.

For the composite systems investigated a practical range for α was established which produces two-way debonding. For fiber volume fraction ranging from 1% to 12%, and aspect ratios (fiber length/fiber diameter) ranging from 40 to 100 for steel fibers, the corresponding range for α would be 5–50. One-way debonding can occur if $\alpha = 0$, (i.e., the strain at the end of the fiber equal to the matrix strain), or with low fiber volume fractions (<0.5%), where the magnitude of interfacial shearing stress at the embedded end of the fiber is very small. These findings agree with those of Leung and Li [13] who have recommended, based on a strength approach, the use of one way debonding for low fiber volume fractions (<0.5) and two-way debonding for high fiber volume fractions.

The extent of fiber debonding at first cracking is relatively lower for DSP than for ordinary FRC as seen in Figures 4 and 5. This difference would lead to larger elastic strain predictions for FRC than for DSP as shown in Figure 7. This difference may be attributable to the very dense microstructure of DSP [22]. Such density is produced by the introduction of microsilica into the matrix in conjunction

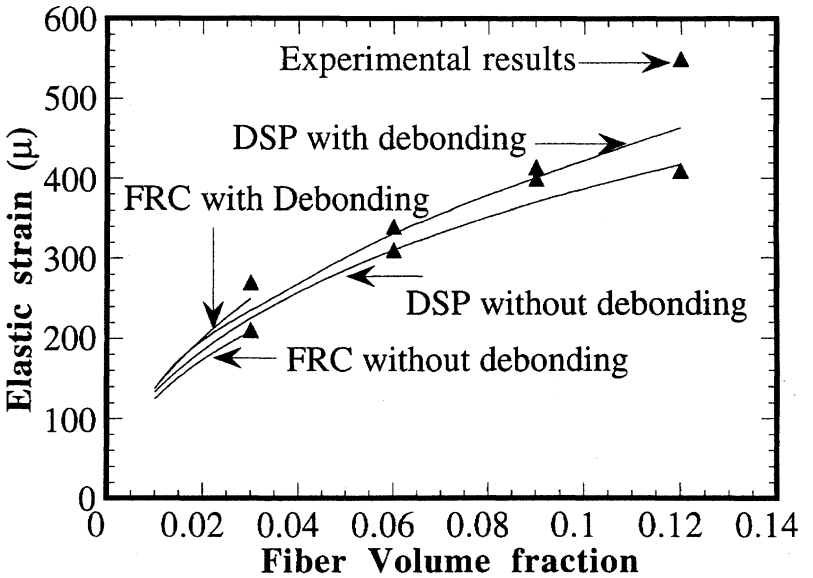

Figure 7. *Effect of partial fiber debonding on elastic strain prediction.*

with a lower water to cement ratio. Table 1 shows that DSP possesses substantial bond strength, two to three times that of ordinary FRC.

CONCLUSIONS

1. Elastic theory was used to predict the extent of debonding on ordinary and high performance FRC's containing discrete fibers. The occurrence of first cracking at the end of elastic range results in two-way debonding.
2. For ordinary strength FRC's containing low volume fraction of fibers (<1%), significant debonding is predicted at first cracking.
3. For a high performance FRC such as a DSP system containing high volume fraction of fibers (>3%), less debonding is predicted at first cracking.
4. For better and improved design of FRC's, designers should incorporate the contribution of partial fiber debonding to elastic strain, as predicted by micro-mechanical models.

NOMENCLATURE

FRC	Fiber reinforced concrete
DSP	Densified small particles
FR-DSP	Fiber reinforced DSP

ν_m Poisson's ratio of the matrix
r the radius of the fiber
R median distance between fibers
ε_{mu} the elastic strain of the composite
V_f volume fraction of fibers
V_{ef} the effective fiber volume fraction, (i.e., half of the nominal value of fiber volume fraction)
γ_m the matrix surface energy
L_f the fiber length
E_f the modulus of elasticity of the fiber
E_m the modulus of elasticity of the matrix
E_c the modulus of elasticity of the composite

$$\alpha = \frac{E_m V_m}{E_f V_{ef}}$$

$$\beta = \frac{L_{tr}}{L_f/2}$$

L_{tr} the fiber transfer length

$$L_{tr} = \frac{d_f \sigma_f}{4\tau}$$

σ_f the fiber stress after cracking

$$\sigma_f = \varepsilon^*_{mu}(1+\alpha)E_f$$

ε^*_{mu} the approximated elastic strain
d_f the fiber diameter
t a constant directional interfacial stress
U the total debonding energy for cylindrical fibers
ΔU the change in the interface debonding energy
G_i the interface debonding energy per unit crack area
L_{db1} the debonded length before cracking
L_{db2} the debonded length after cracking
ΔL_{db} the change in the debonded length

ACKNOWLEDGEMENTS

The authors gratefully acknowledge the financial support of the National Science Foundation Center for Advanced Cement-Based Materials (ACBM) and the support from Aalborg University, Denmark. Thanks to Mr. Sidney Johnson for editorial review.

REFERENCES

1. A. G. Evans and D. B. Marshall, "The Mechanical Behavior of Ceramic Composites," *Acta Metall. Mater.*, 37, 2567, 1989.
2. D. B. Marshall and J. J. Brennan, "High-Strength Silicon Carbide Fiber Reinforced Glass Matrix," *Journal of Materials Science,* 15, 463, 1980.
3. R. J. Kerans and T. A. Parthasarathy, "Failure Mechanisms in Ceramic-Fiber-Matrix Composites," *Journal of American Ceramic Society,* 74, 1585, 1991.
4. R. J. Kerans, R. S. Hay, N. J. Pagano and T. A. Parthasarathy, "The Role of the Fiber-Matrix Interface in Ceramic Composites," *Journal of American Ceramic Society, Bull. 68,* 429, 1989.
5. K. M. Prewo and J. J. Brennan, "Theoretical Analysis of the Fiber Pullout and Pushout Tests," *Journal of Materials Science,* 15, 463, 1980.
6. J. Aveston, and A. Kelly, "Theory of Multiple Fracture of Fibrous Composites," *Journal of Materials Science 8,* pp. 352–362, 1973.
7. J. K. Kim, L. M. Zhou, Y. W. Mai, "Interfacial Debonding and Fiber Pullout Stresses, Part III." *Journal of Materials Science* V. 28, pp. 3923–3930, 1993.
8. H. Stang, Z. Li and S. P. Shah, "Pull-Out Problem: Stress versus Fracture Mechanical Approach." *ASCE Journal of Engineering Mechanics,* V. 116, pp. 2136–2150, 1990.
9. A. E. Naaman, G. Namur, J. M. Alwan and H. Najm, "Fiber Pullout and Bond Slip. I: Analytical Study; II: Experimental Validation," *ASCE Journal of Structural Engineering,* V. 117, pp. 2769–2800, 1991.
10. M. R. Piggott, "Load-Bearing Fiber Composites," Pergamon Press, Oxford, New York, p. 86, 1980.
11. M. Shannag, R. Brincker and W. Hansen, "Interfacial (Fiber-Matrix Properties of High Strength Mortar (150 MPa) from Fiber Pullout," *ACI Materials Journal,* V. 93, No. 5, pp. 480–486, 1996.
12. P. Tjiptobroto, "Tensile Strain Hardening of High Performance Fiber Reinforced Cement Based Composites," Ph.D. dissertation, University of Michigan, Ann Arbor, p. 183, 1991.
13. C. K. Y. Leung and V. C. Li, "Application of a two-way debonding theory to short fiber composites," *Composites,* Vol. 21, No. 4, pp. 305–316, 1990.
14. Y. Shao, Z. Li and P. Shah, "Matrix Cracking and Interface Debonding in Fiber-Reinforced Cement-Matrix Composites." *Advanced Cement Based Materials Journal,* V. 1 No. 2, pp. 55–66, 1993.
15. A. Bentur and S. Mindess, *Fiber Reinforced Cementitious Composites,* Elsevier Science Publisher, p. 430, 1990.
16. P. Balaguru and S. Shah, *Fiber Reinforced Cementitious Composites,* McGraw-Hill Publishing Company Ltd., 1992.
17. P. Tjiptobroto and W. Hansen, "Model for Prediction of the Elastic Strain of Fiber Reinforced Composites Containing High Volume Fractions of Discontinuous Fibers." *ACI Materials Journal,* V. 90, No. 2, 1993.
18. M. Shannag, "Tensile Behavior of Fiber Reinforced DSP," Ph.D. Dissertation, University of Michigan, Ann Arbor, p. 213, 1995.
19. M. Shannag, R. Brincker, and W. Hansen, "Pullout Behavior of Steel Fibers from Cement Based Composites," *Journal of Cement and Concrete Research,* Vol. 27, 1997.
20. P. Lawrence, "Some Theoretical Considerations of Fiber Pullout from an Elastic Matrix," *Journal of Materials Science 7,* pp. 1–6, 1972.
21. V. S. Gopalaratnam and S. P. Shah, "Tensile Fracture of Steel Fiber Reinforced Concrete," *ASCE Engng. Mech. 13,* No. 5, pp. 635–653, 1987.
22. H. H. Bache, "Densified Cement Ultra-Fine Particle-Based Materials," CBL Report No. 40, Aalborg Portland, Aalborg, Denmark, p. 87, 1981.
23. M. Kawamura and S. Igrashi, "Fracture Toughness for Steel Fiber-Cement Paste Interface Zone," *Journal of Materials for Civil Engineers,* Vol. 4, No. 3, 1992.